Atmospheric Research 153 (2015) 19–33

Contents lists available at ScienceDirect

Atmospheric Research

journal homepage: www.elsevier.com/locate/atmos

Effects of turbulence on warm clouds and precipitation with various aerosol concentrations

Hyunho Lee [a], Jong-Jin Baik [a,*], Ji-Young Han [b]

[a] School of Earth and Environmental Sciences, Seoul National University, Seoul 151-742, South Korea
[b] Korea Institute of Atmospheric Prediction Systems, Seoul 156-849, South Korea

ARTICLE INFO

Article history:
Received 6 January 2014
Received in revised form 25 June 2014
Accepted 25 July 2014
Available online 2 August 2014

Keywords:
Turbulence
Collision enhancement
Warm clouds
Precipitation
Bin microphysics

ABSTRACT

This study investigates the effects of turbulence-induced collision enhancement (TICE) on warm clouds and precipitation by changing the cloud condensation nuclei (CCN) number concentration using a two-dimensional dynamic model with bin microphysics. TICE is determined according to the Taylor microscale Reynolds number and the turbulent dissipation rate. The thermodynamic sounding used in this study is characterized by a warm and humid atmosphere with a capping inversion layer, which is suitable for simulating warm clouds. For all CCN concentrations, TICE slightly reduces the liquid water path during the early stage of cloud development and accelerates the onset of surface precipitation. However, changes in the rainwater path and in the amount of surface precipitation that are caused by TICE depend on the CCN concentrations. For high CCN concentrations, the mean cloud drop number concentration (CDNC) decreases and the mean effective radius increases due to TICE. These changes cause an increase in the amount of surface precipitation. However, for low CCN concentrations, changes in the mean CDNC and in the mean effective radius induced by TICE are small and the amount of surface precipitation decreases slightly due to TICE. A decrease in condensation due to the accelerated coalescence between droplets explains the surface precipitation decrease. In addition, an increase in the CCN concentration can lead to an increase in the amount of surface precipitation, and the relationship between the CCN concentration and the amount of surface precipitation is affected by TICE. It is shown that these results depend on the atmospheric relative humidity.

1. Introduction

The effects of turbulence on clouds and precipitation remain an unresolved problem in cloud physics due to their inherent complexity. Turbulence affects not only cloud microphysical processes, such as the collision process and the diffusional processes (condensation, evaporation, deposition, and sublimation), but also mixing and entrainment (Grabowski and Wang, 2013 and references therein). However, observation techniques have not been sufficiently developed to identify the detailed spatio-temporal variability of in-cloud turbulence. It is also challenging to simulate interactions between clouds and turbulent flows in numerical models because simulations that simultaneously consider both turbulent eddies and cloud systems require large computing resources. Therefore, state-of-the-art numerical cloud models are used to parameterize the effects of turbulence. Some recent reviews have provided the current status of this topic (e.g., Khain et al., 2007; Devenish et al., 2012; Grabowski and Wang, 2013).

Direct numerical simulation (e.g., Zhou et al., 2001; Franklin et al., 2005; Ayala et al., 2008) and simulations using turbulent statistical models (e.g., Pinsky et al., 2008) have shown that turbulence increases the collision rate between drops by a few times compared to the collision rate when only considering gravitational collection, which can result in accelerated and increased surface precipitation. By solving the stochastic collection equation, Franklin (2008) demonstrated that turbulence

* Corresponding author.
E-mail address: jjbaik@snu.ac.kr (J.-J. Baik).

http://dx.doi.org/10.1016/j.atmosres.2014.07.026
0169-8095/

substantially affects the evolution of the drop size distribution and can shorten the time required for raindrop formation. Using a large-eddy simulation (LES) model with bulk cloud microphysics, Seifert et al. (2010) showed that turbulence leads to a substantial enhancement in surface precipitation in warm clouds. Benmoshe et al. (2012) investigated the effects of turbulence on deep convective clouds using a bin microphysics cloud model. They showed that the effects of turbulence are opposite to those of cloud condensation nuclei (CCN): turbulence-induced collision enhancement accelerates the formation of the first raindrops while leading to a decrease in the net accumulated surface precipitation in mixed-phase clouds. Riechelmann et al. (2012) developed a new Lagrangian warm cloud model coupled with an LES model and showed that droplets grow more quickly when the effects of turbulence are included. Recently, Wyszogrodzki et al. (2013) examined the effects of turbulence-induced collision enhancement under a specific range of aerosol concentrations in warm clouds using an LES model with bin microphysics and showed an increase in surface precipitation due to turbulence effects. These numerical studies suggest that in-cloud turbulence plays important roles in clouds and precipitation. In this study, we examine whether the effects of turbulence on clouds and precipitation differ as the aerosol concentration varies, focusing on a single warm cloud using a two-dimensional (2-D) dynamical model with bin microphysics. This examination is expected to provide a better understanding of cloud–aerosol interactions and the effects of turbulence on clouds and precipitation.

The numerical model used in this study and the experimental setup are described in Section 2. The simulation results are presented and discussed in Section 3. A summary and conclusions are provided in Section 4.

2. Model description and experimental setup

The Hebrew University Cloud Model (HUCM) is used for this study. A detailed description of the model is provided by Khain and Sednev (1996) and Khain et al. (2000, 2004). The model is a 2-D cloud model that uses a bin method to treat the hydrometeor and aerosol size distributions. Each size distribution is represented by 43 mass-doubling bins. The in-cloud nucleation process is represented using a semi-Lagrangian method (Khain et al., 2000). Some improvements on the treatment of the diffusional processes for highly variable supersaturation and a remapping algorithm that conserves additional moments of the cloud particle size distribution are described by Khain et al. (2008). The scavenging process and the regeneration process of aerosols due to the evaporation of droplets are not included.

The results of Pinsky et al. (2008) are used in this study to include turbulence-induced collision enhancement (hereafter, TICE) between small droplets in the numerical model. TICE is determined as a function of the Taylor microscale Reynolds number and the turbulent dissipation rate. One advantage of this method is that it can be applied for relatively high turbulent dissipation rates (up to 0.1 m^{-2} s^{-3}) and Reynolds numbers (up to 20,000). The model uses the 1.5th order turbulent closure to prognostically calculate the turbulent kinetic energy (Skamarock et al., 2008; Benmoshe et al., 2012); the Taylor microscale Reynolds number and the turbulent dissipation rate are calculated using the computed turbulent kinetic energy. Because the model is 2-D and the grid size is not small enough to explicitly resolve turbulence, it is inherently not possible to precisely describe turbulent flows. However, despite this limitation, Benmoshe et al. (2012) used the same cloud model and presented a detailed structure of cloud turbulence and demonstrated the capability of this model to investigate the effects of TICE on clouds and precipitation.

The thermodynamic sounding used by Ogura and Takahashi (1973) is adopted to simulate a single warm shallow cloud (Fig. 1). One important feature of this sounding is the existence of a strong inversion layer between $z = 3$ km and $z = 3.4$ km, which prevents the growth of clouds above this layer. Another important characteristic is a humid atmosphere compared to that of previous studies (e.g., Xue et al., 2008; vanZanten et al., 2011). The water vapor mixing ratio at the surface is 17.4 g kg^{-1}, and the water vapor mixing ratio averaged over the lowest 1 km is 14.8 g kg^{-1}. The horizontal wind speed is set to zero at the surface and increases linearly with height to 5 m s^{-1} at $z = 4$ km. The wind speed remains constant above 4 km. The temperature at the bottom of the inversion layer is 5.3°C (Fig. 1); thus, only warm clouds are simulated in this study.

It is assumed that all aerosols can serve as CCN according to their radii and the ambient supersaturation. The aerosol number concentration is constant below $z = 2$ km and decreases exponentially with height above 2 km; the e-folding depth is 2 km. Following Khain et al. (2000), the aerosol size distribution $N(r_a)$ is formulated using the Köhler equation (Köhler, 1936; Pruppacher and Klett, 1997) and the Twomey equation (Twomey, 1959), which is given by

$$\frac{dN}{d\ln r_a} = \frac{3}{2} N_0 k \left(\frac{4A^3}{27Br_a^3} \right)^{k/2}. \quad (1)$$

Here, r_a is the aerosol particle radius, N_0 is the CCN number concentration at 1% supersaturation, k is a constant, A is a temperature-dependent coefficient that is related to the curvature effect, and B is a constant that is related to the solution effect. The value of k is specified as 0.5. The numerical experiments are performed for aerosol number concentrations of $N_0 = 30$, 100, 300, 1000, and 3000 cm^{-3}.

The domain size is 51.2 km in the horizontal and 8 km in the vertical. A damping layer is included from $z = 5$ km to the top of the model domain. The horizontal and vertical grid spacing is 50 m. The time step is 1 s except for the diffusional processes (0.1 s). The integration time is 2 h. Convection is initiated using a specified low-level heating of 0.01 K s^{-1} for the first 100 s of the simulations. Additional numerical experiments are performed by varying the intensity of the initial heating rate to obtain an ensemble. Although the number of numerical experiments is small, the results (not shown) show that the overall structures of the simulated clouds are not substantially altered due to changes in the low-level heating. Therefore, only the results using the reference heating intensity (0.01 K s^{-1}) are shown in the following sections.

3. Results and discussion

3.1. Macroscopic structures

Fig. 2 depicts the liquid water path (LWP, calculated using both cloud droplets and raindrops), rainwater path (RWP),

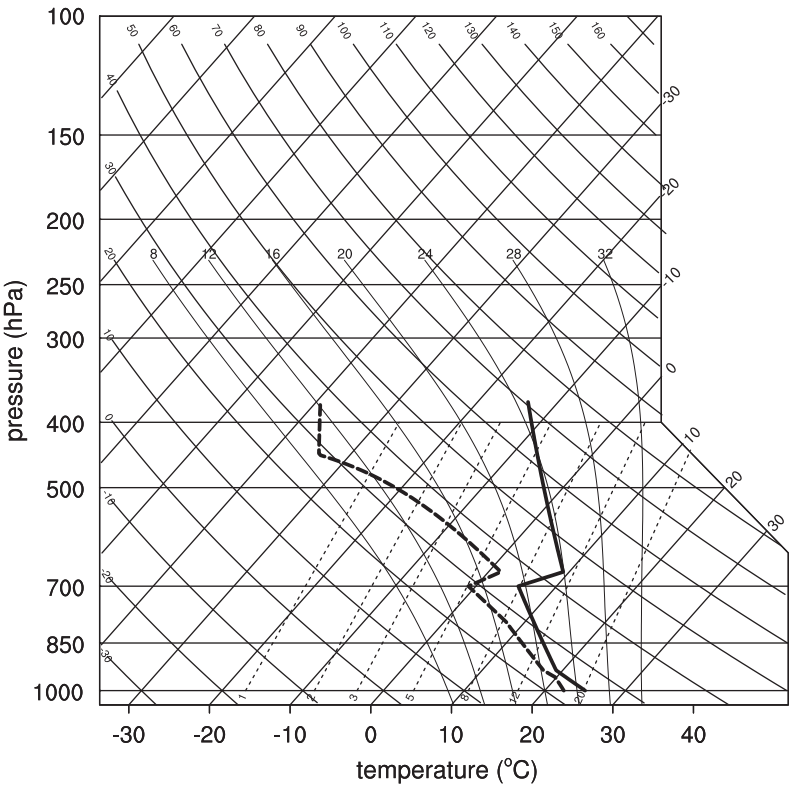

Fig. 1. Thermodynamic sounding used in this study, which is adopted from Ogura and Takahashi (1973). Thick solid and dashed lines indicate the air temperature and dew point temperature, respectively.

surface precipitation rate, and accumulated surface precipitation time series for $N_0 = 30$, 100, 300, 1000, and 3000 cm^{-3} with and without TICE. Because all liquid drops are represented in one hydrometeor category in the model, drops with a radius smaller than 0.1 mm are considered to be cloud droplets; larger drops are considered to be raindrops. The LWP, RWP, surface precipitation rate, and the accumulated surface precipitation are averaged over $x = 13$–23 km, which encompasses the simulated cloud in each simulation. Although the model is integrated for 2 h, only the growth and decay of the initial clouds are the foci of this analysis; clouds that appear after the decay of the initial cloud are excluded in the analysis.

The LWP time series demonstrates that TICE and changes in the CCN concentration alter the LWP after approximately 20 min. An increase in the CCN concentration tends to increase the LWP. Although the differences in the LWP induced by TICE are generally less than those induced by changes in the CCN concentration, TICE tends to decrease the LWP during the early stage of cloud development. One reason for this LWP decrease is that TICE enhances coalescence between small droplets, which accelerates the formation of large drops, ultimately increasing the fallout of drops. Another reason for this LWP decrease is that the enhanced coalescence between small droplets reduces the bulk condensation due to the reduced sum of the drop radii.

The RWP and surface precipitation rate exhibit more variance than the LWP with respect to changes in the CCN concentration and TICE (Fig. 2b–d). A few previous studies have shown that the RWP and surface precipitation rate are more sensitive than the LWP to model configurations and environmental conditions (e.g., Arabas and Shima, 2013). TICE produces an earlier onset of raindrop formation and surface precipitation. The effect of TICE on the onset of surface precipitation becomes larger as the CCN concentration increases. Specifically, the onset of surface precipitation is accelerated by 1 min for $N_0 = 30$ cm^{-3} and 17 min for $N_0 = 3000$ cm^{-3}. The CCN concentration is also known to affect the onset of surface precipitation (e.g., Albrecht, 1989; Han et al., 2012). In this study, surface precipitation begins 19 min earlier for $N_0 = 30$ cm^{-3} than for $N_0 = 3000$ cm^{-3} in the cases that include TICE. Under the conditions considered in this study, the acceleration in the onset of surface precipitation due to TICE (17 min) is comparable to the acceleration caused by a decrease in the CCN concentration (19 min).

Interestingly, TICE causes an increase in the RWP and the amount of surface precipitation only when $N_0 \geq 300$ cm^{-3}. Previous studies have shown that TICE always increases the amount of surface precipitation in warm clouds, i.e., even for $N_0 < 300$ cm^{-3}, due to the accelerated collisions between small droplets (e.g., Seifert et al., 2010; Wyszogrodzki et al., 2013). However, in this study, the effect of TICE on the accumulated surface precipitation depends on the CCN concentration, which differs from the results of previous studies. When $N_0 = 3000$ cm^{-3}, an average of 0.2 mm and 0.05 mm of surface precipitation falls over the first hour of the simulations in the cases with and without TICE, respectively. However, when $N_0 = 30$ cm^{-3}, TICE decreases the amount of surface

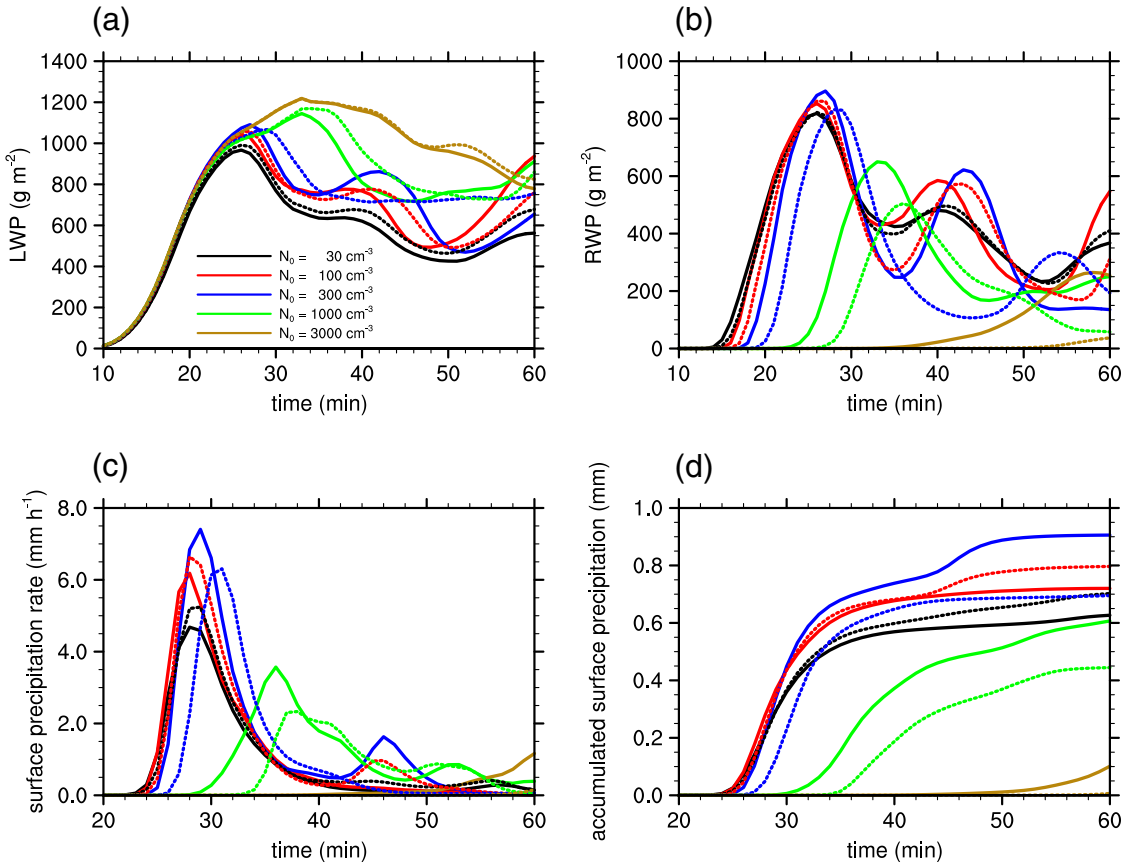

Fig. 2. (a) Liquid water path (LWP) (g m^{-2}), (b) rainwater path (RWP) (g m^{-2}), (c) surface precipitation rate (mm h^{-1}), and (d) accumulated surface precipitation (mm) time series averaged over x = 13–23 km for N_0 = 30, 100, 300, 1000, and 3000 cm^{-3}. Solid and dashed lines correspond to the cases with and without TICE, respectively.

precipitation by 11%. This decrease for $N_0 = 30$ cm^{-3} is small compared to the increase for $N_0 = 3000$ cm^{-3} (a factor of four). The mechanism that causes these differences is examined in Section 3.3.

3.2. Microscopic structures

The vertical distribution of the mean effective radius r_e, which is defined as

$$r_e = \frac{\int_0^\infty r^3 f(r) dr}{\int_0^\infty r^2 f(r) dr}, \quad (2)$$

where r is the drop radius and $f(r)$ is the drop size distribution, is presented in Fig. 3. In the following analysis, only grid points at which the cloud drop number concentration (CDNC) ≥20 cm^{-3} (except for $N_0 = 30$ cm^{-3}, in which CDNC ≥15 cm^{-3}) are used for averaging (e.g., Benmoshe et al., 2012; Arabas and Shima, 2013). Although several studies have used only small droplets for calculating r_e to directly compare with observations obtained using, e.g., forward scattering spectrometer probes (e.g., Brenguier et al., 1998; Arabas and Shima, 2013), this study uses all drops to calculate r_e because the effect of TICE on the growth of small droplets into large drops is explicitly analyzed. Therefore, the mean effective radius presented in this study is slightly larger than that reported in previous studies.

Fig. 3 shows that the mean effective radius increases with height and exhibits a maximum directly below the cloud top, which largely agrees with the results of previous studies (e.g., Arabas and Shima, 2013). The height at which the mean effective radius reaches its maximum depends on the specific cases; however, the maximum typically occurs between z = 2 km and z = 3 km. The maximum mean effective radius is approximately 130 μm when $N_0 = 30$ cm^{-3} and decreases as N_0 increases. Moreover, the maximum mean effective radius is less than 20 μm when N_0 is greater than 1000 cm^{-3}.

TICE is expected to increase the drop sizes due to the accelerated collisions between small droplets. However, when N_0 = 30 and 100 cm^{-3}, the changes in the mean effective radius that are caused by TICE are not distinct. When $N_0 = 30$ cm^{-3}, the mean effective radius is slightly larger only in z ~ 1–2 km when TICE is included compared to the case without TICE; for $N_0 = 100$ cm^{-3}, the same is true

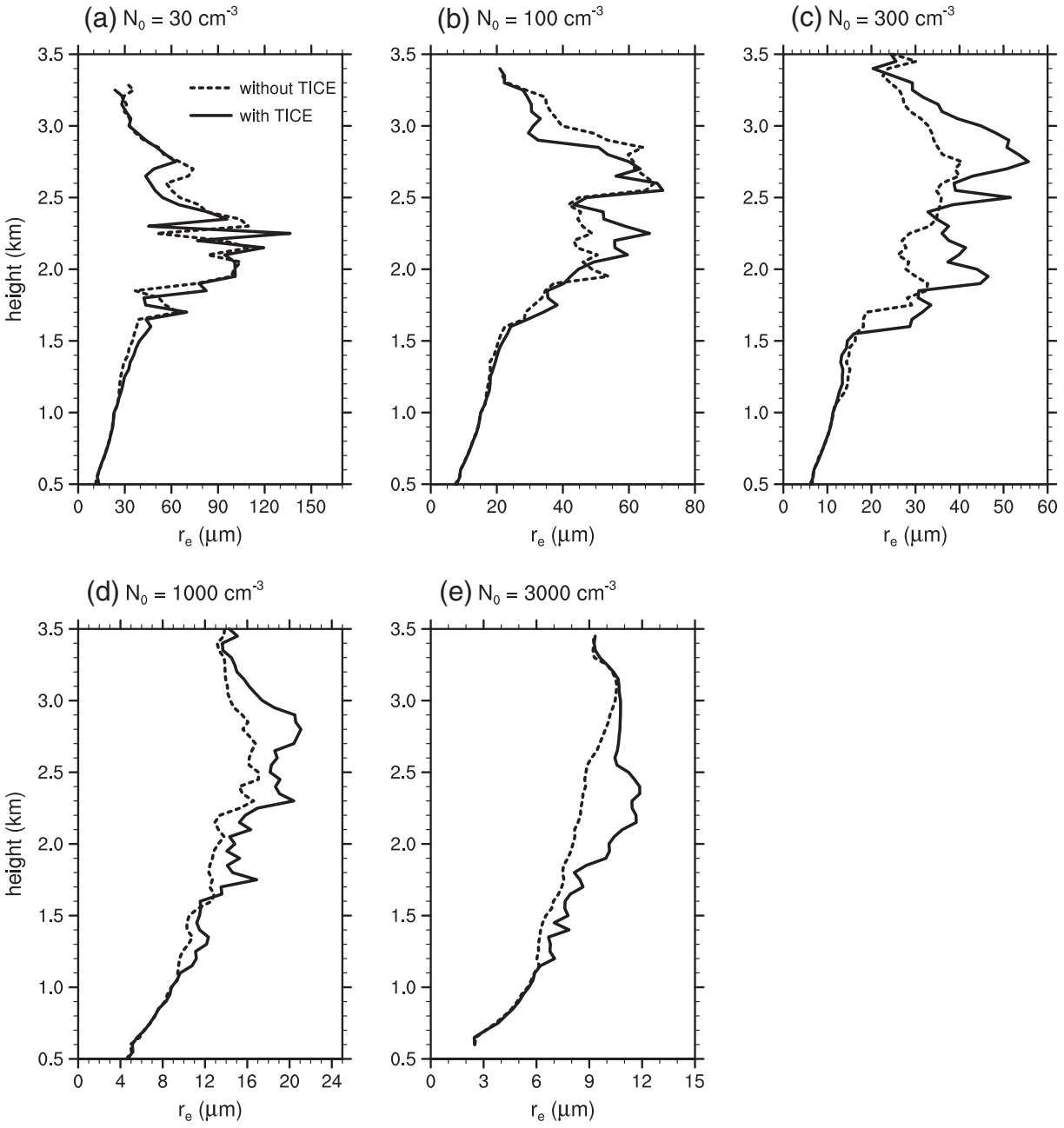

Fig. 3. Vertical distribution of mean effective radius r_e (μm) averaged over the grid points in which the cloud drop number concentration (CDNC) ≥20 cm^{-3} except for $N_0 = 30$ cm^{-3} (CDNC ≥15 cm^{-3}) for $N_0 =$ (a) 30, (b) 100, (c) 300, (d) 1000, and (e) 3000 cm^{-3}. r_e is averaged over $t =$ (a), (b), and (c) 10–30 min, (d) 15–35 min, and (e) 35–55 min. Solid and dotted lines correspond to the cases with and without TICE, respectively.

only in $z \sim 1.5$–2.5 km (Fig. 3a and b). However, the increase in the mean effective radius becomes smaller or even completely diminishes above these layers. Generally, the enlarged drop radius that is caused by TICE is more pronounced as the CCN concentration increases. When $N_0 = 3000$ cm^{-3}, the mean effective radius is enlarged by nearly 50% in $z =$ 2–2.5 km as a result of TICE. Although the model is designed such that TICE always accelerates the coalescence of droplets, the enlarged drop radius that is caused by TICE is only well pronounced for high CCN concentrations, i.e., $N_0 \geq 300$ cm^{-3}, in this study. The effect is not certain for low CCN concentrations.

Fig. 4 shows the vertical distribution of the mean CDNC for various CCN concentrations. Except when $N_0 = 30$ cm^{-3}, the mean CDNC tends to decrease with height. TICE is expected to reduce the mean CDNC due to the accelerated coalescence of droplets. However, TICE produces only very small changes in

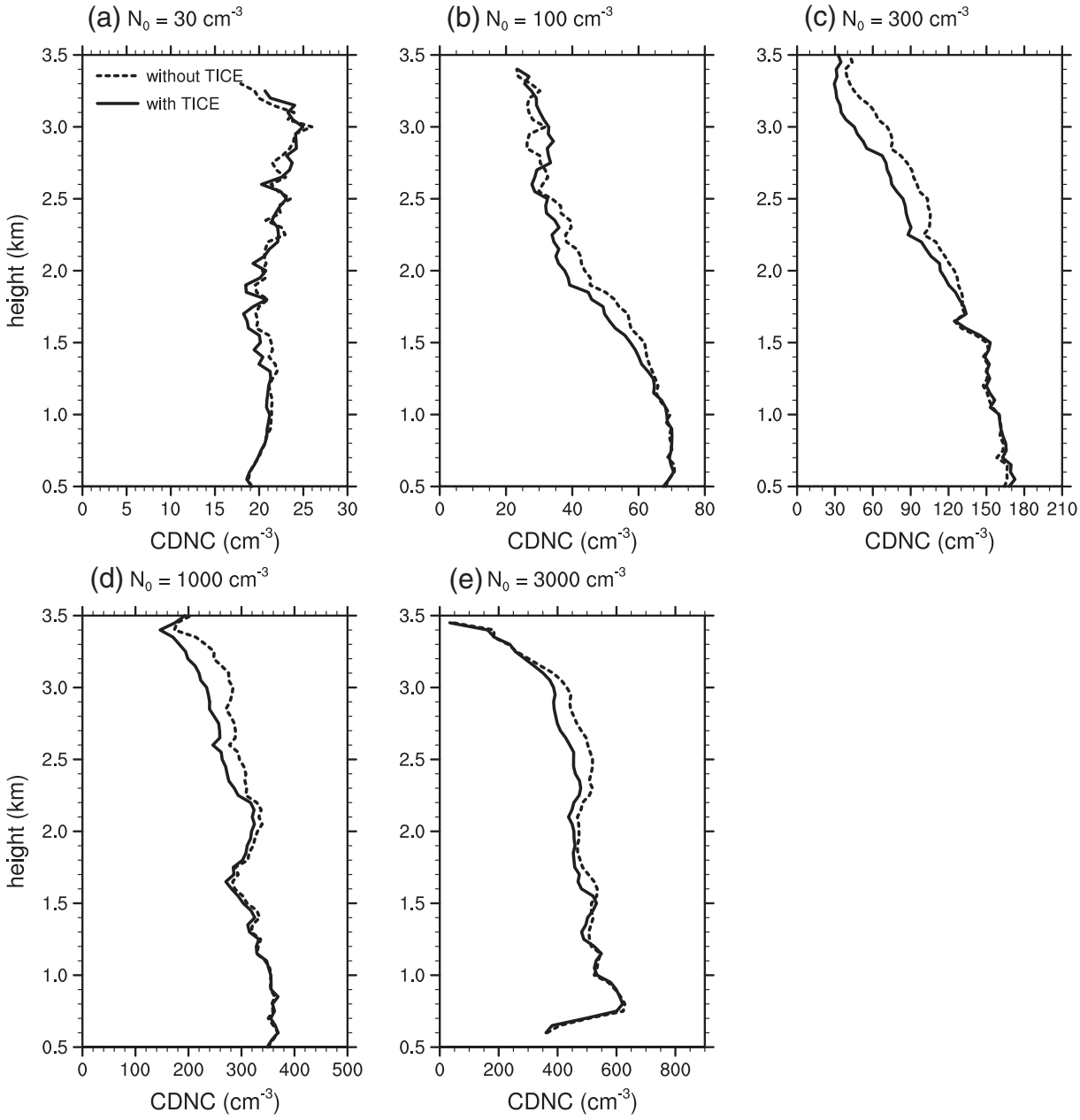

Fig. 4. The same as in Fig. 3 but for CDNC (cm^{-3}).

CDNC when $N_0 = 30\ cm^{-3}$, and the change in the CDNC caused by TICE depends on height when $N_0 = 100\ cm^{-3}$. The reduction in the CDNC is more pronounced when $N_0 \geq 300\ cm^{-3}$.

By analyzing the mean effective radius and the CDNC, it is concluded that TICE exhibits only a small effect on accelerating the growth of droplets by coalescence for low CCN concentrations. Because TICE affects the coalescence of relatively small droplets, if droplets are capable of growing via vapor diffusion to sizes that are sufficient for coalescence without TICE, the coalescence acceleration caused by TICE becomes small. Due to the humid atmosphere that is considered in this study, the diffusional growth of small droplets is sufficiently vigorous such that the droplets grow to sizes at which coalescence is effective even without TICE for low CCN concentrations. Therefore, the differences in the mean effective radius and in the mean CDNC between the cases with and without TICE are small.

To evaluate the model suitability for investigating the effects of TICE, the instantaneous turbulent dissipation rate ε, Taylor microscale Reynolds number Re_λ, and liquid water content (LWC) fields for $N_0 = 100\ cm^{-3}$ at $t = 15$ min and the turbulent dissipation rate time series are all presented in Fig. 5. Observational studies have revealed that a typical Re_λ is ~10^4 and a typical ε is in the range 10^{-4}–$10^{-2}\ m^{-2}\ s^{-3}$ for shallow

convective clouds or cumuli (Jonas, 1996; Pruppacher and Klett, 1997; Siebert et al., 2006, 2010). However, Re_λ and ε have been known to exhibit a very high temporal and spatial variability (Shaw, 2003; Benmoshe et al., 2012). In this study, the instantaneous fields of ε and Re_λ also exhibit a high spatial variability (Fig. 5a and b). Comparatively high values of ε appear near the cloud top, where the wind shear is large. Fig. 5a and c shows the collocation of regions in which large ε and LWC appear. This result agrees with the results of previous studies (e.g., Seifert et al., 2010; Benmoshe et al., 2012; Khain et al., 2013) and suggests that TICE is generally large in areas with high drop concentrations. Therefore, TICE efficiently affects the coalescence of small droplets. Fig. 5d indicates that the turbulent dissipation rate is not largely affected by the CCN concentration and TICE. The turbulent dissipation rate increases to ~10^{-2} m^{-2} s^{-3} during the early stage of cloud development and then decreases before remaining at ~10^{-3} m^{-2} s^{-3} after the decay of the initial cloud in each simulation, which is within the range suggested in previous studies.

3.3. Effects of TICE on surface precipitation

Fig. 2d shows that TICE increases the amount of surface precipitation when $N_0 \geq 300$ cm^{-3}, whereas TICE decreases the amount of surface precipitation when $N_0 \leq 100$ cm^{-3}. Therefore, the cases in which $N_0 = 1000$ cm^{-3} and $N_0 = 100$ cm^{-3} are chosen to further investigate the different effects of TICE on the amount of surface precipitation. The case of $N_0 = 1000$ cm^{-3} represents the relatively high CCN concentration cases, and the case of $N_0 = 100$ cm^{-3} represents the relatively low CCN concentration cases.

Previous studies have suggested that the rapid growth of cloud droplets to raindrops is the primary mechanism by which TICE increases the amount of surface precipitation (e.g., Franklin, 2008). Therefore, the cloud water content and rainwater content are examined to determine how TICE contributes to the increase in the amount of surface precipitation for high CCN concentrations. Figs. 6 and 7 show the cloud water content and rainwater content fields at $t = 27$ min and $t = 32$ min for $N_0 = 1000$ cm^{-3}, respectively. At $t = 27$ min, the cloud water content is smaller and the rainwater content is larger in the case with TICE compared to the case without TICE. This result is simply related to the enhanced coalescence between cloud droplets, resulting in the more rapid growth of cloud droplets into raindrops. At $t = 32$ min, the cloud water content remains smaller and the rainwater content remains larger in the case with TICE compared to the case without TICE (Fig. 7). Because cloud droplets are quite small for high CCN concentrations, the droplets are less likely to coalesce into raindrops when only gravitational collisions are represented. However, in the case with TICE, cloud droplets coalesce and grow into raindrops more easily. Consequently, the rainwater content and the amount of surface precipitation increase.

Fig. 8 shows the rainwater fraction time series for the cases with and without TICE for $N_0 = 1000$ cm^{-3}. Here, the rainwater

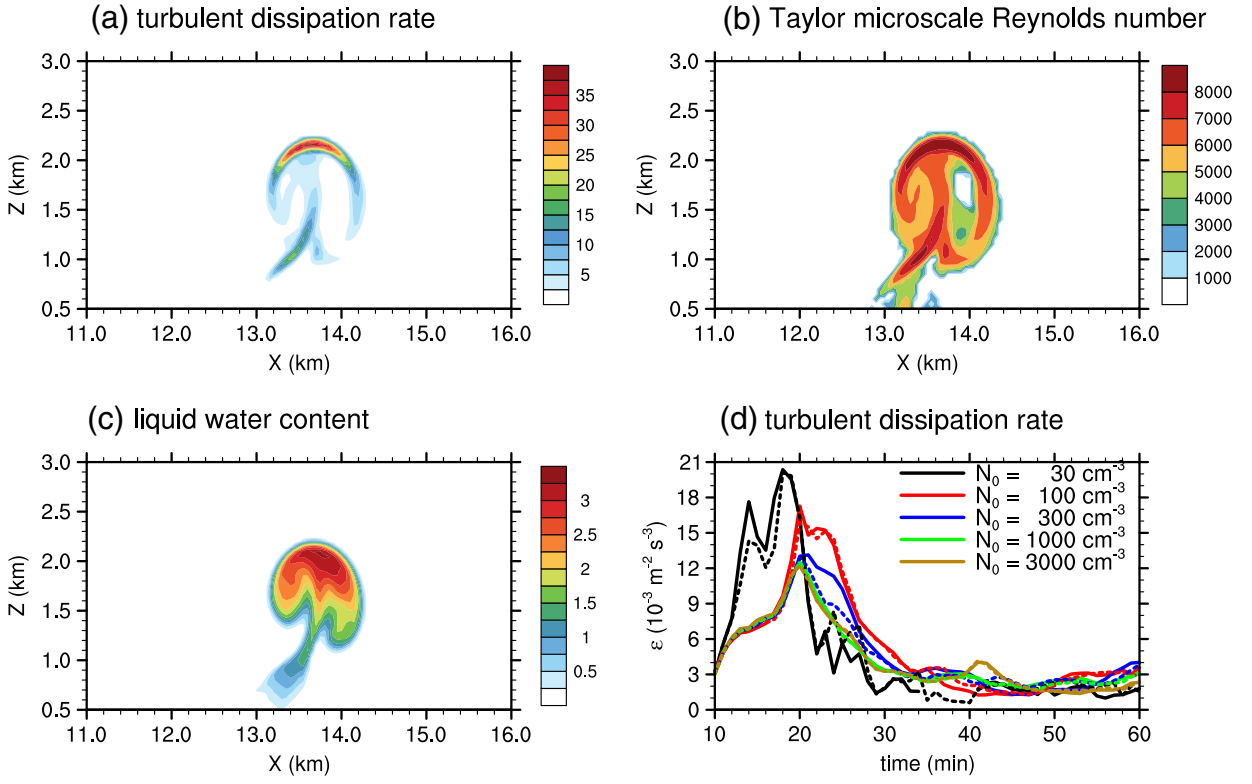

Fig. 5. (a) Turbulent dissipation rate (10^{-3} m^{-2} s^{-3}), (b) Taylor microscale Reynolds number, (c) liquid water content (g m^{-3}) fields at $t = 15$ min for $N_0 = 100$ cm^{-3} when TICE is included, and (d) averaged turbulent dissipation rate time series. Solid and dashed lines in (d) correspond to the cases with and without TICE, respectively.

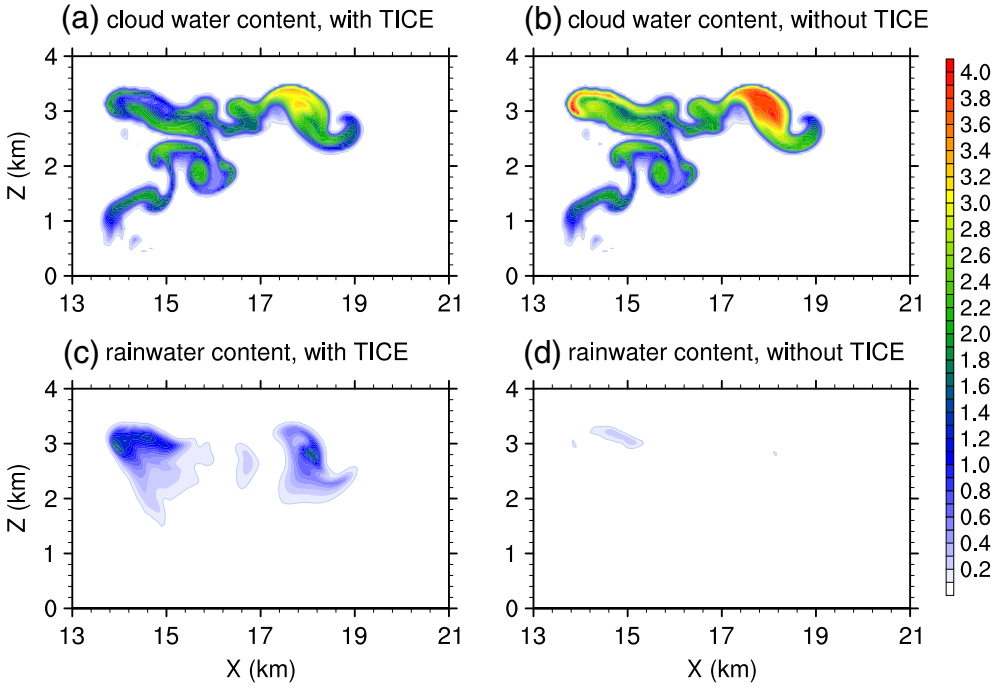

Fig. 6. (a) Cloud water content (g m^{-3}) and (c) rainwater content (g m^{-3}) fields at $t = 27$ min for $N_0 = 1000$ cm^{-3} when TICE is included. (b) and (d) are the same as (a) and (c), respectively, but when TICE is not included.

fraction is defined as the ratio of the total rainwater content to the total liquid water content (i.e., the cloud water content plus rainwater content) in the entire domain. The maximum rainwater fraction is 0.57 at $t = 34$ min in the case with TICE; a smaller maximum value (0.44 at $t = 37$ min) is observed in the case without TICE. This result demonstrates that the growth of cloud droplets into raindrops is both delayed and suppressed in the case without TICE for $N_0 = 1000$ cm^{-3}.

In contrast to the high CCN concentration results, TICE slightly decreases the amount of surface precipitation for low

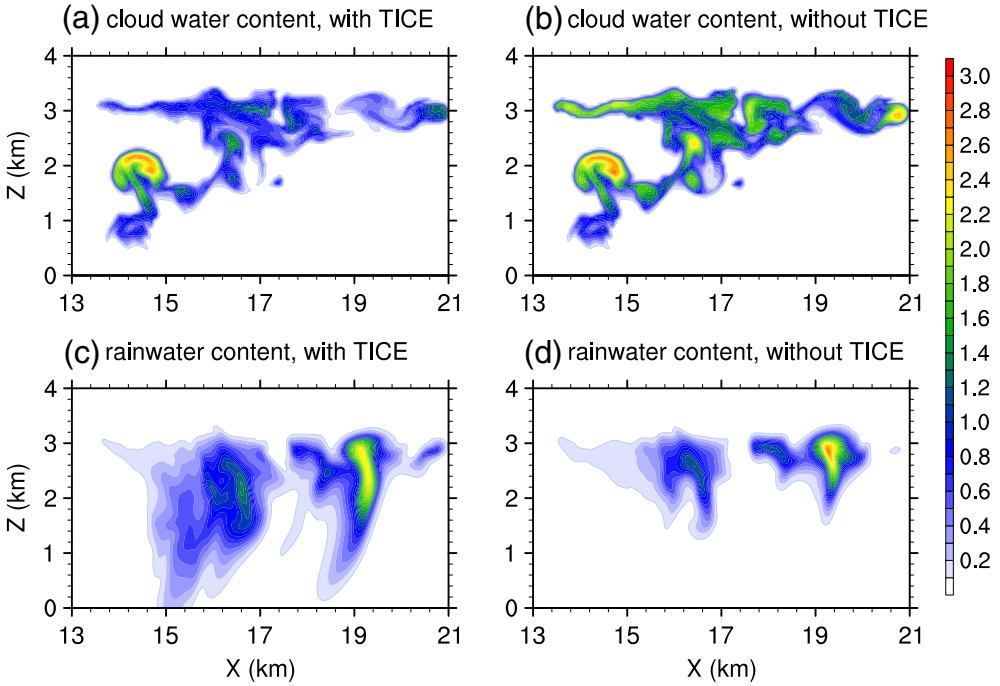

Fig. 7. The same as in Fig. 6 but at $t = 32$ min.

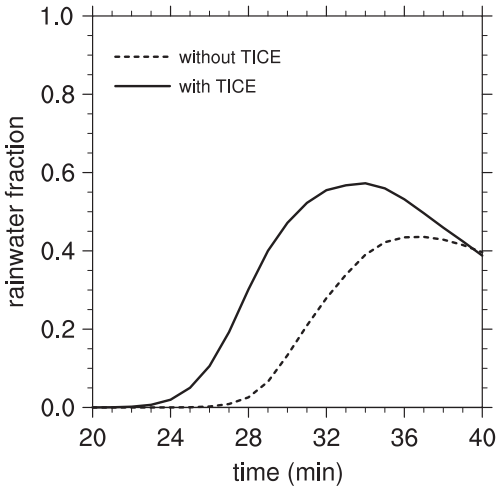

Fig. 8. The rainwater fraction time series in the cases with and without TICE for $N_0 = 1000\ \mathrm{cm}^{-3}$.

CCN concentrations. To examine how TICE decreases the amount of surface precipitation for low CCN concentrations, the cloud water content and rainwater content fields at $t =$ 20 min and $t = 25$ min for $N_0 = 100\ \mathrm{cm}^{-3}$ are depicted in Figs. 9 and 10, respectively. Because of the accelerated onset of surface precipitation that is caused by a reduction in the CCN concentration, the selected times are different from those selected for the $N_0 = 1000\ \mathrm{cm}^{-3}$ analysis (Fig. 2c and d).

At $t = 20$ min (Fig. 9), the cloud water content is smaller and the rainwater content is larger in the case with TICE compared to the case without TICE; this result is the same as for $N_0 = 1000\ \mathrm{cm}^{-3}$. However, at $t = 25$ min (Fig. 10), the cloud water content and rainwater content differences between the two cases are small. The rainwater content in the case with TICE is larger only below $z \sim 1.6$ km (Fig. 10e and f). Above $z \sim 1.6$ km, the rainwater content in the case with TICE is smaller than that in the case without TICE. These changes are because raindrops in the case with TICE fall into the lower layer, while cloud droplets in the case without TICE coalesce into raindrops in the upper layer at $t = 20$–25 min.

Fig. 11 shows the rainwater fraction time series for $N_0 = 100\ \mathrm{cm}^{-3}$. Rainwater is produced approximately 1 min earlier in the case with TICE compared to the case without TICE, and the rainwater fraction is larger until $t = 26$ min in the case with TICE. However, the rate at which the rainwater fraction increases is similar in the two cases. The rainwater fractions are nearly the same after $t = 26$ min. The decrease in the rainwater fraction after $t = 26$ min is primarily due to the fallout of raindrops to the surface. The maximum rainwater fraction in the case with TICE (0.82) is approximately the same as in the case without TICE.

The accumulated surface precipitation is slightly smaller in the cases with TICE than in the cases without TICE for low CCN concentrations despite the accelerated formation of raindrops and the subsequent earlier onset of surface precipitation. To explain this result, the diffusional processes are examined because the collision–coalescence process and the breakup process do not affect the total water content. A comparison between condensation and evaporation shows that the condensation process dominates the evaporation process during the developing stage of the cloud in the individual cases (not shown). Therefore, the differences in the total liquid water mass primarily originate from the condensation process.

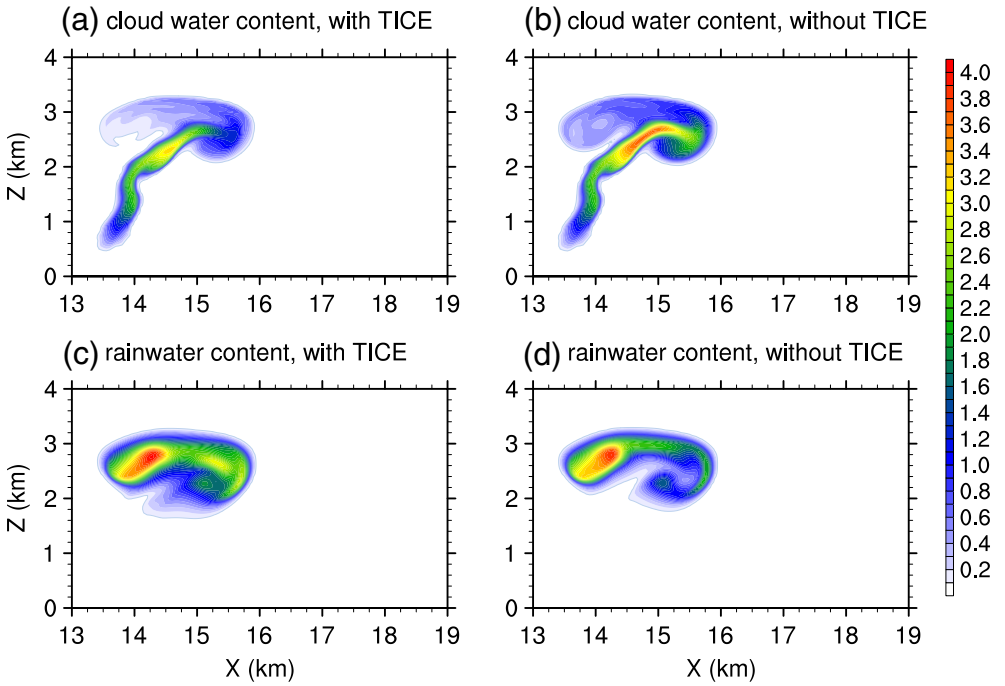

Fig. 9. (a) Cloud water content ($\mathrm{g\ m}^{-3}$) and (c) rainwater content ($\mathrm{g\ m}^{-3}$) fields at $t = 20$ min for $N_0 = 100\ \mathrm{cm}^{-3}$ when TICE is included. (b) and (d) are the same as (a) and (c), respectively, but when TICE is not included.

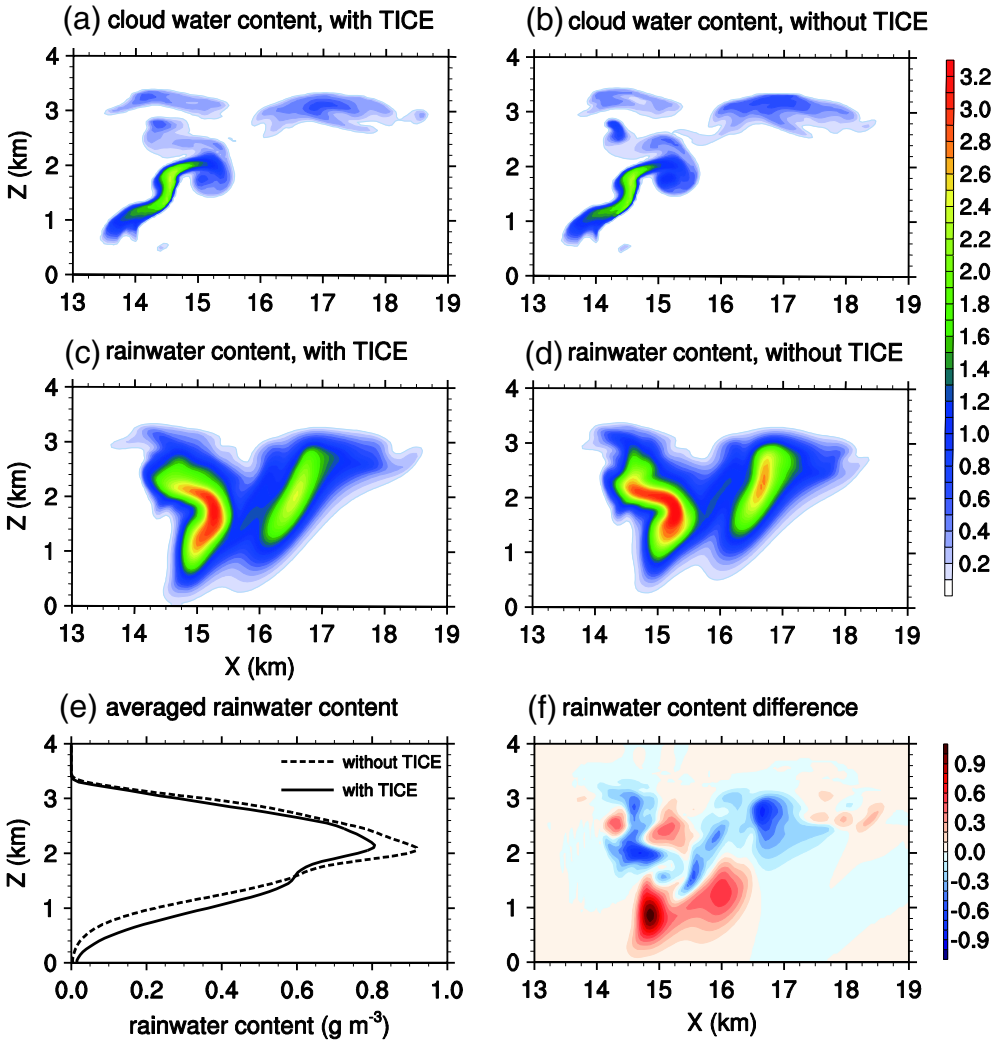

Fig. 10. (a)–(d) the same as in Fig. 9 but at $t = 25$ min, (e) vertical profiles of rainwater content (g m^{-3}) averaged over $x = 13$–19 km, and (f) the differences in rainwater content due to TICE at $t = 25$ min for $N_0 = 100$ cm^{-3}.

The vertical profile of the horizontally averaged condensational heating rate for $t = 20$–25 min and $N_0 = 100$ cm^{-3} is plotted in Fig. 12a. This figure shows that the condensation rate in the case with TICE is smaller than in the case without TICE. This difference is most noticeable in $z \sim 2$–3 km, where most cloud droplets are concentrated (see Fig. 9). The rapid decrease in the condensation rate above $z = 3$ km is due to the existence of the inversion layer and the resultant constraint on upward motion. Fig. 12b shows the domain-averaged condensational heating rate time series. The condensation rate in the case with TICE is smaller than that in the case without TICE. The total condensation for $t =$ 0–25 min, which is calculated by integrating the condensation rate over the period, is smaller in the case with TICE than in the case without TICE by 2.6%. This decrease in the total condensation due to TICE is caused by the early coalescence of small droplets. Accelerated collisions between small droplets increase the mean drop radius and decrease the sum of the drop radii if the total liquid water content is assumed to be constant. Therefore, the total condensation decreases because it is proportional to the sum of the drop radii.

The decrease in the total condensation may also be caused by the reduced liquid water content because TICE decreases the liquid water content via the accelerated coalescence and fallout of drops during the early stage of cloud development. By comparing the total condensation per unit liquid water content, it is revealed that the decrease in the sum of the drop radii has a larger effect than the liquid water content decrease on the reduced total condensation (not shown). However, it is certain that the reduced liquid water content plays a partial role in reducing the total condensation. The reduced liquid water content, which is caused by the accelerated fallout of large drops, should be considered together with the decrease in the sum of the drop radii to account for the reduction in the total condensation due to TICE.

Fig. 13 shows the drop size distributions for $N_0 = 100$ and 1000 cm^{-3}. The distributions are derived in the rain shaft

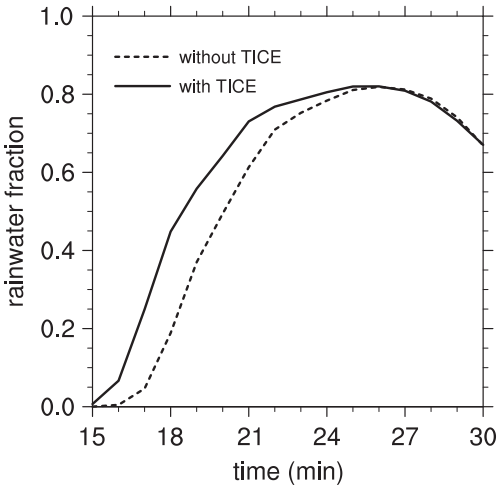

Fig. 11. The rainwater fraction time series in the cases with and without TICE for $N_0 = 100\ \mathrm{cm}^{-3}$.

area, i.e., where the rainwater mixing ratio $\geq 0.5\ \mathrm{g\ kg}^{-1}$ and $z < 0.5$ km, following previous observational studies (e.g., Baker et al., 2009). The time instant is selected to approximately coincide with the surface precipitation rate maximum in each case. When $N_0 = 100\ \mathrm{cm}^{-3}$, although the difference in the two cases is very small, the number concentration of large drops ($r > 600$ μm) is smaller in the case with TICE than in the case without TICE. However, when $N_0 = 1000\ \mathrm{cm}^{-3}$, the number concentration of large drops is 10–1000 times higher in the case with TICE than in the case without TICE. The number concentration of small droplets is also higher in the case with TICE than in the case without TICE.

Thus far, our analysis has focused on the cloud microphysical properties. It is known that differences in the amount of surface precipitation also arise from differences in cloud dynamical properties, such as updraft intensity or cloud top height (e.g., Han et al., 2012; Wyszogrodzki et al., 2013). To investigate the effects of TICE on cloud dynamical properties,

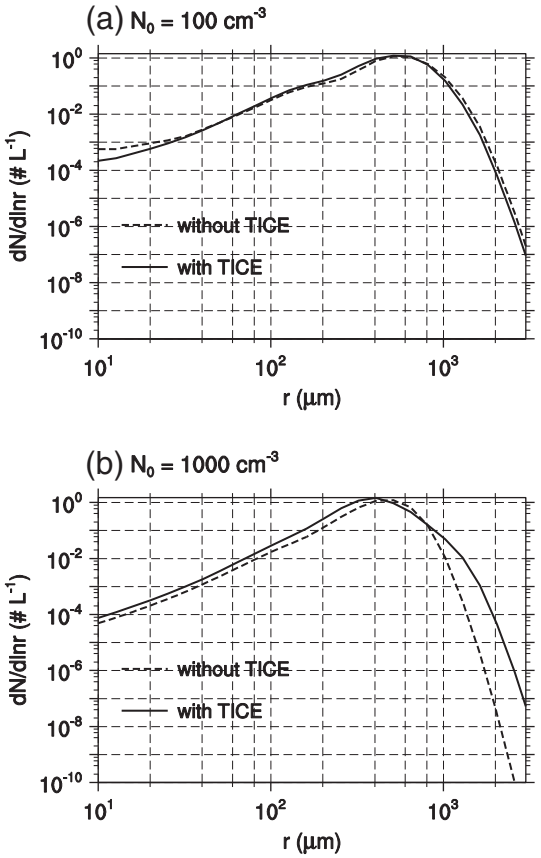

Fig. 13. Drop size distributions (# L^{-1}) in the rain shaft area (where rainwater mixing ratio $\geq 0.5\ \mathrm{g\ kg}^{-1}$ and $z < 0.5$ km) (a) at $t = 30$ min for $N_0 = 100\ \mathrm{cm}^{-3}$ and (b) at $t = 40$ min for $N_0 = 1000\ \mathrm{cm}^{-3}$.

the vertical velocity is analyzed. The vertical distribution of the mean vertical velocity is displayed in Fig. 14. Referring to Fig. 4b and c, when $N_0 = 100\ \mathrm{cm}^{-3}$ and $N_0 = 300\ \mathrm{cm}^{-3}$, the mean

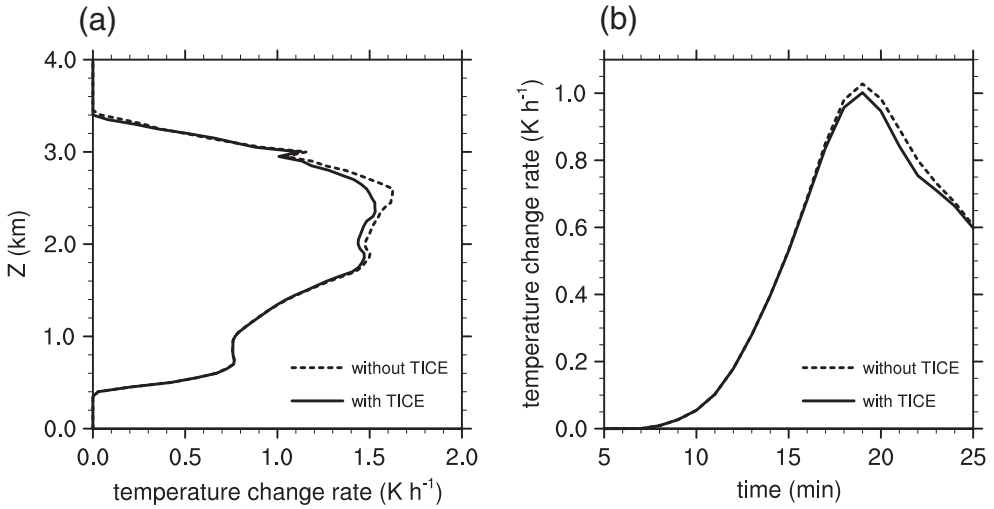

Fig. 12. (a) Vertical profile of the horizontally averaged condensational heating rate (K h^{-1}) for $t = 20$–25 min and (b) the domain-averaged condensational heating rate time series in the cases with and without TICE for $N_0 = 100\ \mathrm{cm}^{-3}$.

vertical velocity appears to be related to the CDNC because a decrease in the CDNC decreases the condensational heat release. However, such a relationship is not applicable for the other CCN concentrations. Moreover, the mean vertical velocity near the cloud base, which is an important dynamical property, is not altered by TICE. Because of the strong inversion layer between $z = 3$ km and $z = 3.4$ km, the difference in the mean vertical velocity cannot alter the cloud top height. The importance of this result was previously noted by Wyszogrodzki et al. (2013). These results indicate that the differences in cloud microphysical properties exert a large control on changes in the amount of surface precipitation in this study and that the vertical velocity differences appear to have a relatively small role. However, this conclusion may originate from the numerical method used in this study because convection is initiated by an externally imposed heating. Further detailed studies are required to investigate the effects of TICE on cloud dynamical properties.

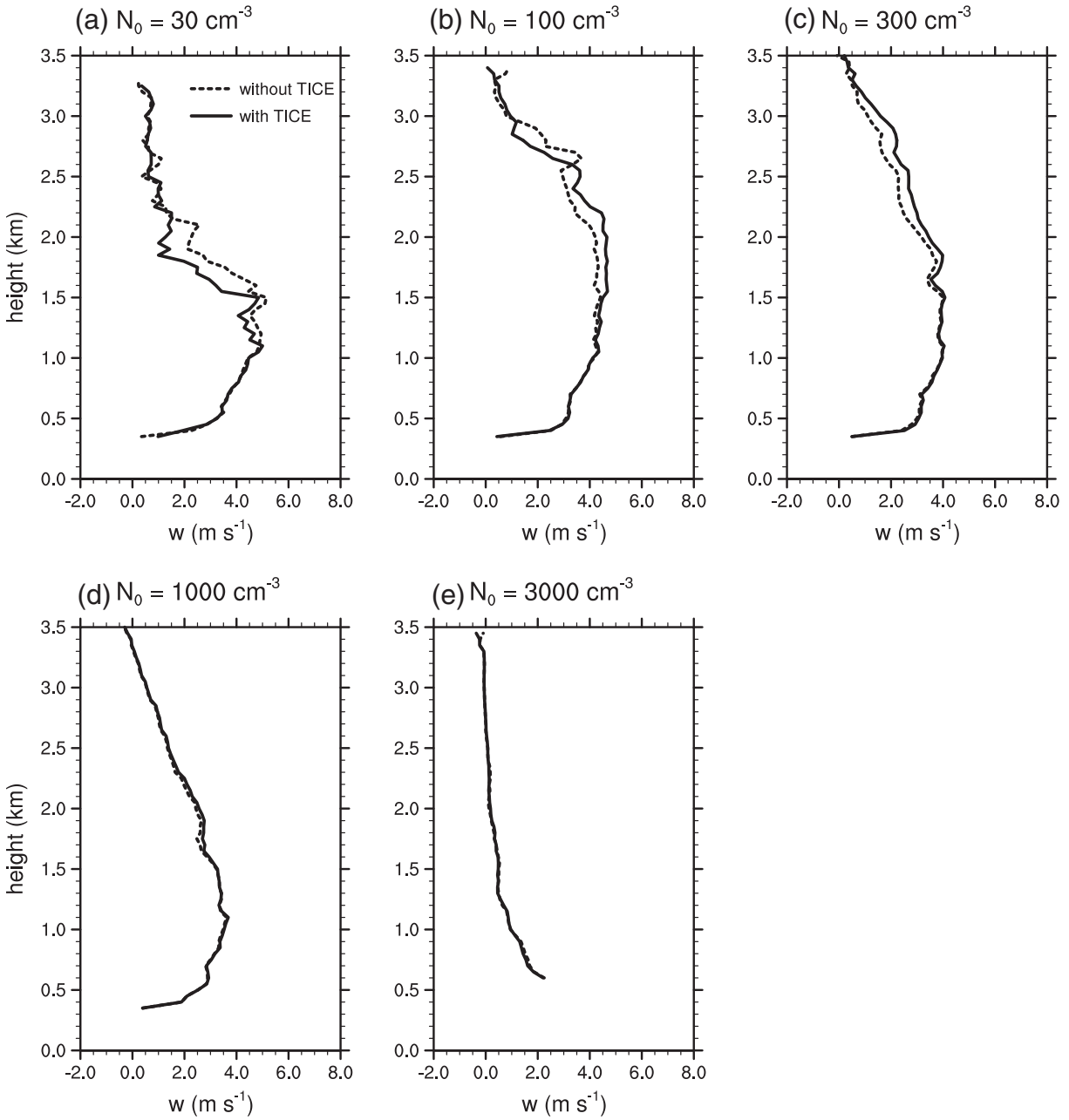

Fig. 14. Vertical distribution of vertical velocity ($m\,s^{-1}$) averaged over the grid points in which the cloud drop number concentration (CDNC) $\geq 20\ cm^{-3}$ except for $N_0 = 30\ cm^{-3}$ (CDNC $\geq 15\ cm^{-3}$) for $N_0 =$ (a) 30, (b) 100, (c) 300, (d) 1000, and (e) 3000 cm^{-3}. The vertical velocity is averaged over $t =$ (a), (b), and (c) 10–30 min, (d) 15–35 min, and (e) 35–55 min. Solid and dotted lines correspond to the cases with and without TICE, respectively.

3.4. Comparisons with results of previous studies

A few recent studies (e.g., Seifert et al., 2010; Wyszogrodzki et al., 2013) have also investigated the effects of TICE on clouds, especially on warm clouds. These studies concluded that the amount of surface precipitation always increases due to TICE. However, in this study, changes in the amount of surface precipitation depend on the CCN concentration. The amount of surface precipitation decreases slightly due to TICE for low CCN concentrations.

The numerical models used in the individual studies are different. Wyszogrodzki et al. (2013) used an LES model with bin microphysics in which the bin resolution (mass-doubling every three bins) is higher than that used in this study (mass-doubling every one bin). They obtained the same conclusions (i.e., the amount of surface precipitation always increases due to TICE) using both an idealized 2-D and a realistic 3-D setup. Seifert et al. (2010) used another LES model with bulk microphysics and obtained nearly the same conclusions. Therefore, it seems that the number of spatial dimensions and the model complexity for treating the drop size distribution have only a small effect on the conclusions.

To investigate potential causes for the different results of this study compared to previous studies, additional numerical experiments are performed. The relative humidity is set to 70% at the surface and 77% near the cloud base, which is 15% lower relative to the original environmental conditions. The water vapor mixing ratio at the surface is 14.4 g kg^{-1}, and the water vapor mixing ratio averaged over the lowest 1 km is 12.2 g kg^{-1}.

The surface precipitation rate time series for the modified environmental conditions and N_0 = 30, 100, 300, 1000, and 3000 cm^{-3} are depicted in Fig. 15. The amount of surface precipitation is considerably smaller compared to the simulations performed with the original environmental conditions, i.e., the amount of surface precipitation is strongly affected by humidity. For example, the maximum surface precipitation rate decreases by more than 90% compared to the simulations performed using the original environmental conditions for N_0 = 30 cm^{-3}, and the extent of the decrease increases rapidly as N_0 increases. Moreover, even in the cases with TICE, there is no surface precipitation when $N_0 \geq 1000$ cm^{-3}.

The amount of surface precipitation always increases due to TICE under the modified environmental conditions; this conclusion corresponds to the findings of the previous studies. In the original environmental conditions of this study, the amount of surface precipitation decreases due to TICE for low CCN concentrations because the small droplets can grow via vapor diffusion such that they efficiently coalesce without TICE. In drier environmental conditions, such growth of small droplets by vapor diffusion is suppressed. Therefore, the decreased surface precipitation due to TICE does not appear.

Another important aspect of this study is that the amount of surface precipitation increases with increasing CCN concentration for low CCN concentrations (when N_0 is less than 300 cm^{-3} with TICE and less than 100 cm^{-3} without TICE) under the original environmental conditions. The increased surface precipitation with increasing aerosol concentration does not appear in the simulations performed with the modified drier environmental conditions.

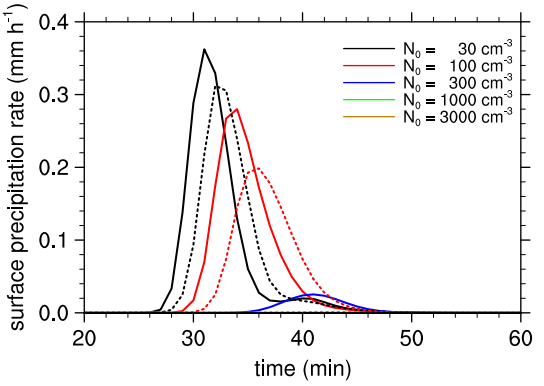

Fig. 15. Surface precipitation rate time series (mm h^{-1}) averaged over x = 13–23 km in drier environmental conditions (a relative humidity of 70% at the surface) for N_0 = 30, 100, 300, 1000, and 3000 cm^{-3}. Solid and dashed lines correspond to the cases with and without TICE, respectively.

It is widely accepted that an increase in aerosol concentration suppresses the amount of surface precipitation in warm clouds (e.g., Albrecht, 1989; Rosenfeld, 1999; Xue and Feingold, 2006; Xue et al., 2008). Although an increase in aerosol concentration reduces surface precipitation due to reduced droplet sizes in warm clouds is regarded as "conventional wisdom", it is frequently found that an increase in the aerosol concentration increases the surface precipitation up to a certain aerosol concentration (e.g., Givati and Rosenfeld, 2004; Seifert and Beheng, 2006; Fan et al., 2009; Carrió et al., 2010; Carrió and Cotton, 2011; Lakshmana et al., 2012) or monotonically increases the surface precipitation (e.g., Lee et al., 2010; Han et al., 2012; Lee and Feingold, 2013) in deep convective clouds. Khain (2009) reviewed the relationships between aerosol concentration and the amount of surface precipitation and showed that the decrease in the amount of surface precipitation with increasing aerosol concentration generally occurs in dry and continental environments or in warm and shallow cumuli. This study suggests that even in warm clouds, the relationship between aerosol concentration and surface precipitation also depends on the humidity of the atmosphere.

The results of this study largely agree with those of Benmoshe et al. (2012), which show that the effects of TICE on surface precipitation are opposite to the effects of increasing aerosol concentration on surface precipitation. In this study, surface precipitation decreases (increases) due to TICE when the aerosol concentration is with the range in which an increase in the aerosol concentration increases (decreases) the surface precipitation.

4. Summary and conclusions

This study investigated the effects of turbulence on warm clouds and the resulting precipitation. Numerical experiments were conducted using various aerosol number concentrations with a 2-D dynamic model that incorporates bin microphysics. The cloud model accounts for turbulence-induced collision enhancement (TICE). The Taylor microscale Reynolds number and the turbulent dissipation rate, which are used to determine TICE, are calculated using the turbulent kinetic energy that is predicted in the model.

In all simulations, TICE enhances coalescence between small droplets, which accelerates the onset of surface precipitation and reduces the liquid water path during the early stage of cloud development. The cloud microstructure, including the drop effective radius and cloud drop number concentration, is also affected by TICE. Although TICE is expected to increase the mean effective radius and decrease the mean cloud drop number concentration via enhanced coalescence, such results are found only for high CCN concentrations. This result is because the growth of droplets via vapor diffusion is sufficiently vigorous in low CCN concentrations and highly humid environments to allow the droplets to grow to sizes at which they can coalesce efficiently. Therefore, the effect of TICE on the amount of surface precipitation depends on the CCN concentration. For high CCN concentrations, TICE substantially increases the amount of surface precipitation, because it is less likely for small droplets to grow into large drops under high CCN concentrations without the assistance of TICE, and TICE enhances the coalescence of cloud droplets into raindrops. However, for low CCN concentrations, TICE slightly decreases the amount of surface precipitation because the early coalescence of small droplets due to TICE decreases the total condensation. These results are summarized in a schematic diagram in Fig. 16. Furthermore, these results depend strongly on the atmospheric relative humidity. In the drier environmental condition, TICE always increases the accumulated surface precipitation even for low CCN concentrations, which is different with the results obtained from the original environmental conditions. This is because the growth of small droplets into large drops under low CCN concentrations via vapor diffusion is not active in the drier environmental condition.

Although this study demonstrates that including TICE is essential for obtaining a better understanding of clouds and precipitation, there are several features that are not considered in this study. Specifically, 3-D large-eddy simulation (LES) or direct numerical simulation (DNS) can provide more realistic turbulence variables, such as the Taylor microscale Reynolds number and the turbulent dissipation rate. Moreover, turbulence affects many processes in addition to the collision process. Turbulence enhances mixing between clouds and their surrounding environment, which can cause a substantial decrease in the liquid water content (e.g., Gerber et al., 2008). The diffusional processes are also partially affected by turbulence (e.g., Vaillancourt et al., 2002; Lanotte et al., 2009). In addition, the extent to which turbulence enhances collisions between ice particles and between drops and ice particles remains highly uncertain. Further research that considers all of the above aspects would lead to a better understanding of the effects of turbulence on clouds and precipitation.

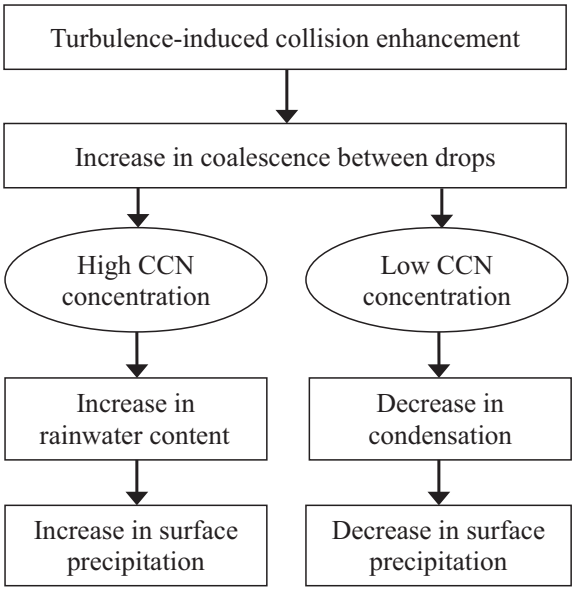

Fig. 16. Schematic diagram that shows the different effects of TICE on the amount of surface precipitation for high and low CCN concentrations.

Acknowledgments

The authors are grateful to two anonymous reviewers for providing valuable comments on this work. The first and second authors were supported by the Korea Meteorological Administration Research and Development Program under grant CATER 2012-6030 and also by the National Research Foundation of Korea (NRF) grant funded by the Korea Ministry of Science, ICT and Future Planning (MSIP) (No. 2011-0017041). The third author was supported by the R&D project on the development of Korea's global numerical weather prediction systems of Korea Institute of Atmospheric Prediction Systems (KIAPS) funded by the Korea Meteorological Administration (KMA). This work was supported by the National Institute of Supercomputing and Networking/Korea Institute of Science and Technology Information with supercomputing resources including technical support (no. KSC-2012-C3-15).

References

Albrecht, B.A., 1989. Aerosols, cloud microphysics, and fractional cloudiness. Science 245, 1227–1230.

Arabas, S., Shima, S.-I., 2013. Large eddy simulations of trade-wind cumuli using particle-based microphysics with Monte-Carlo coalescence. J. Atmos. Sci. 70, 2768–2777.

Ayala, O., Rosa, B., Wang, L.-P., 2008. Effects of turbulence on the geometric collision rate of sedimenting droplets. Part II: theory and parameterization. New J. Phys. 10, 075016.

Baker, B., Mo, Q., Lawson, R., O'Connor, D., Korolev, A., 2009. Drop size distributions and the lack of small drops in RICO rain shafts. J. Appl. Meteorol. Climatol. 48, 616–623.

Benmoshe, N., Pinsky, M., Pokrovsky, A., Khain, A., 2012. Turbulent effects on the microphysics and initiation of warm rain in deep convective clouds: 2-D simulations by a spectral mixed-phase microphysics cloud model. J. Geophys. Res. 117, D06220.

Brenguier, J.-L., Bourrianne, T., Coelho, A., Isbert, J., Peytavi, R., Trevarin, D., Weschler, P., 1998. Improvements of droplet size distribution measurements with the Fast-FSSP (forward scattering spectrometer probe). J. Atmos. Ocean. Technol. 15, 1077–1090.

Carrió, G.G., Cotton, W.R., 2011. Urban growth and aerosol effects on convection over Houston. Part II: dependence of aerosol effects on instability. Atmos. Res. 102, 167–174.

Carrió, G.G., Cotton, W.R., Cheng, W.Y.Y., 2010. Urban growth and aerosol effects on convection over Houston. Part I: the August 2000 case. Atmos. Res. 96, 560–574.

Devenish, B.J., Bartello, P., Brenguier, J.L., Collins, L.R., Grabowski, W.W., IJzermans, R.H.A., Malinowski, S.P., Reeks, M.W., Vassilicos, J.C., Wang, L.-P., Warhaft, Z., 2012. Droplet growth in warm turbulent clouds. Q. J. R. Meteorol. Soc. 138, 1401–1429.

Fan, J., Yuan, T., Comstock, J.M., Ghan, S., Khain, A., Leung, L.R., Li, Z., Martins, V.J., Ovchinnikov, M., 2009. Dominant role by vertical wind shear in regulating aerosol effects on deep convective clouds. J. Geophys. Res. 114, D22206.

Franklin, C.N., 2008. A warm rain microphysics parameterization that includes the effect of turbulence. J. Atmos. Sci. 65, 1795–1816.
Franklin, C.N., Vaillancourt, P.A., Yau, M.K., Bartello, P., 2005. Collision rates of cloud droplets in turbulent flows. J. Atmos. Sci. 62, 2451–2466.
Gerber, H.E., Frick, G.M., Jensen, J.B., Hudson, J.G., 2008. Entrainment, mixing, and microphysics in trade-wind cumulus. J. Meteorol. Soc. Jpn. 86A, 87–106.
Givati, A., Rosenfeld, D., 2004. Quantifying precipitation suppression due to air pollution. J. Appl. Meteorol. 43, 1038–1056.
Grabowski, W.W., Wang, L.-P., 2013. Growth of cloud droplets in a turbulent environment. Annu. Rev. Fluid Mech. 45, 293–324.
Han, J.-Y., Baik, J.-J., Khain, A.P., 2012. A numerical study of urban aerosol impacts on clouds and precipitation. J. Atmos. Sci. 69, 504–520.
Jonas, P.R., 1996. Turbulence and cloud microphysics. Atmos. Res. 40, 283–306.
Khain, A.P., 2009. Note on state-of-the-art investigations of aerosol effects on precipitation: a critical review. Environ. Res. Lett. 4, 015004.
Khain, A.P., Sednev, I., 1996. Simulation of precipitation formation in the Eastern Mediterranean coastal zone using a spectral microphysics cloud ensemble model. Atmos. Res. 43, 77–110.
Khain, A.P., Ovtchinnikov, M., Pinsky, M., Pokrovsky, A., Krugliak, H., 2000. Notes on the state-of-the-art numerical modeling of cloud microphysics. Atmos. Res. 55, 159–224.
Khain, A.P., Pokrovsky, A., Pinsky, M., Seifert, A., Phillips, V., 2004. Simulation of effects of atmospheric aerosols on deep turbulent convective clouds using a spectral microphysics mixed-phase cumulus cloud model. Part I: model description and possible applications. J. Atmos. Sci. 61, 2963–2982.
Khain, A.P., Pinsky, M., Elperin, T., Kleeorin, N., Rogachevskii, I., Kostinski, A., 2007. Critical comments to results of investigations of drop collisions in turbulent clouds. Atmos. Res. 86, 1–20.
Khain, A.P., BenMoshe, N., Pokrovsky, A., 2008. Factors determining the impact of aerosols on surface precipitation from clouds: an attempt at classification. J. Atmos. Sci. 65, 1721–1748.
Khain, A.P., Prabha, T.V., Benmoshe, N., Pandithurai, G., Ovchinnikov, M., 2013. The mechanism of first raindrops formation in deep convective clouds. J. Geophys. Res. Atmos. 118, 9123–9140.
Köhler, H., 1936. The nucleus in and the growth of hygroscopic droplets. Trans. Faraday Soc. 32, 1152–1161.
Lakshmana, R.V., Krishna, S.S.V.S.R., Murty, K.P.R.V., 2012. A comprehensive study of aerosols around Visakhapatnam, a coastal region, India. Ecol. Environ. Conserv. 18, 53–59.
Lanotte, A.S., Seminara, A., Toschi, F., 2009. Cloud droplet growth by condensation in homogeneous isotropic turbulence. J. Atmos. Sci. 66, 1685–1697.
Lee, S.S., Feingold, G., 2013. Aerosol effects on the cloud-field properties of tropical convective clouds. Atmos. Chem. Phys. 13, 6713–6726.
Lee, S.S., Donner, L.J., Penner, J.E., 2010. Thunderstorm and stratocumulus: how does their contrasting morphology affect their interactions with aerosols? Atmos. Chem. Phys. 10, 6819–6837.
Ogura, Y., Takahashi, T., 1973. The development of warm rain in a cumulus cloud. J. Atmos. Sci. 30, 262–277.
Pinsky, M., Khain, A.P., Krugliak, H., 2008. Collisions of cloud droplets in a turbulent flow. Part V: application of detailed tables of turbulent collision rate enhancement to simulation of droplet spectra evolution. J. Atmos. Sci. 65, 357–374.
Pruppacher, H.R., Klett, J.D., 1997. Microphysics of Clouds and Precipitation, 2nd ed. Kluwer Academic Publishers.
Riechelmann, T., Noh, Y., Raasch, S., 2012. A new method for large-eddy simulations of clouds with Lagrangian droplets including the effects of turbulent collision. New J. Phys. 14, 065008.
Rosenfeld, D., 1999. TRMM observed first direct evidence of smoke from forest fires inhibiting rainfall. Geophys. Res. Lett. 26, 3105–3108.
Seifert, A., Beheng, K., 2006. A two-moment cloud microphysics parameterization for mixed-phase clouds. Part II: maritime vs. continental deep convective storms. Meteorol. Atmos. Phys. 92, 67–82.
Seifert, A., Nuijens, L., Stevens, B., 2010. Turbulence effects on warm-rain autoconversion in precipitating shallow convection. Q. J. R. Meteorol. Soc. 136, 1753–1762.
Shaw, R.A., 2003. Particle–turbulence interactions in atmospheric clouds. Annu. Rev. Fluid Mech. 35, 183–227.
Siebert, H., Lehmann, K., Wendisch, M., 2006. Observations of small-scale turbulence and energy dissipation rates in the cloudy boundary layer. J. Atmos. Sci. 61, 1451–1466.
Siebert, H., Shaw, R.A., Warhaft, Z., 2010. Statistics of small-scale velocity fluctuations and internal intermittency in marine stratocumulus clouds. J. Atmos. Sci. 67, 262–273.
Skamarock, W.C., Klemp, J.B., Dudhia, J., Gill, D.O., Barker, D.M., Duda, M.G., Huang, X.-Y., Wang, W., Powers, J.G., 2008. A description of the advanced research WRF version 3. NCAR Technical Note, NCAR/TN–475 + STR, NCAR.
Twomey, S., 1959. The nuclei of natural cloud formation. Part II: the supersaturation in natural clouds and the variation of cloud droplet concentration. Pure Appl. Geophys. 43, 243–249.
Vaillancourt, P.A., Yau, M.K., Bartello, P., Grabowski, W.W., 2002. Microscopic approach to cloud droplet growth by condensation. Part II: turbulence, clustering, and condensational growth. J. Atmos. Sci. 59, 3421–3435.
vanZanten, M.C., Stevens, B., Nuijens, L., Siebesma, A.P., Ackerman, A.S., Burnet, F., Cheng, A., Couvreux, F., Jiang, H., Khairoutdinov, M., Kogan, Y., Lewellen, D.C., Mechem, D., Nakamura, K., Noda, A., Shipway, B.J., Slawinska, J., Wang, S., Wyszogrodzki, A., 2011. Controls on precipitation and cloudiness in simulations of trade-wind cumulus as observed during RICO. J. Adv. Model. Earth Syst. 3, M06001.
Wyszogrodzki, A.A., Grabowski, W.W., Wang, L.-P., Ayala, O., 2013. Turbulent collision–coalescence in maritime shallow convection. Atmos. Chem. Phys. 13, 8471–8487.
Xue, H., Feingold, G., 2006. Large-eddy simulations of trade wind cumuli: investigation of aerosol indirect effects. J. Atmos. Sci. 63, 1605–1622.
Xue, H., Feingold, G., Stevens, B., 2008. Aerosol effects on clouds, precipitation, and the organization of shallow cumulus convection. J. Atmos. Sci. 65, 392–406.
Zhou, Y., Wexler, A.S., Wang, L.-P., 2001. Modelling turbulent collision of bidisperse inertial particles. J. Fluid Mech. 433, 77–104.